TECHNICAL PAPER

Hybrid fused filament fabrication for manufacturing of Al microfilm reinforced PLA structures

Ranvijay Kumar[1] · Jasgurpreet Singh Chohan[2] · Raman Kumar[2] · Aniket Yadav[2] · Piyush[2] · Narinder Singh[3]

Abstract

The quality of 3D printed thermoplastic structures mainly depends upon the various aspects of deposition pattern, processing conditions, and layer bonding. The incomplete layer-to-layer adhesion during the additive manufacturing process is the most critical issue since thermoplastics are bad heat conductors. In this study, aluminum (Al) microfilms have been deposited to promote the adhesion between the additive layers. The composite structures (as per ASTM D 695) of polylactic acid thermoplastic were manufactured by fused filament fabrication (FFF) process and consecutively reinforced with Al spray. The composite structures were subjected to compressive loading to investigate the influence of input process variables like; in-between microfilm layers (1–5 layers), bed temperature (60–100 °C), and infill percentage (40–100%). The results of the study suggested that using microfilm in-between additive layers is a promising technique for improving the compressive properties. The compressive strength has been observed maximum by performing FFF with 3 layers of Al microfilm, 70% of infill percentage, and 100 °C bed temperature. The results are supported by scanning electron microscopy, energy-dispersive spectroscopy, and differential scanning calorimeter analysis. An optimization study was successfully conducted using the analytic hierarchy process, which predicted the optimum parameter settings based on the relative importance of each response variable.

Keywords Al microfilm · PLA · Hybrid FFF · Compressive strength · Reinforced structures

1 Introduction

AM is a digital fabrication processes through which parts having complex shapes can be formed at lower cost and time as compared to conventional manufacturing techniques [1]. AM is gaining popularity due to its application in almost every sector for preparing prototypes in engineering [2], the biomedical industry [3], electronic industry [4], and ceramic industry [5] and educational models [6]. The AM techniques are classified under seven broad categories, i.e., material extrusion [7], binder jetting, directed energy deposition [8], material jetting, powder bed fusion, sheet lamination [9], and vat photopolymerization as per ASTM F2792-12a [10]. FFF is one of the most economical and popular material extrusion techniques due to material flexibility, portability, and easy operation [11]. The FFF processes cover the wide range of materials such as metals [12], polymers [13], wood [14], ceramics [15], biomaterials [16], food materials [17], and their composites. Among available materials used for FFF printers, PLA and acrylonitrile butadiene styrene (ABS) are commonly used. Nowadays, the additive manufacturing of metals, nonmetals, and reinforced polymeric materials is very common to attain the desired properties of products [18, 19]. The product made using FFF has different surface finish, density, tensile strength, compressive strength, and weight, which depends on various parameters, i.e., nozzle speed, infill density, bed temperature, and infill pattern [20]. The characteristics of reinforcements added to thermoplastic material are significant factors that influence the mechanical and thermal properties of parts fabricated by the FFF process. The combination of PLA, polymethyl methacrylate

✉ Ranvijay Kumar
  ranvijayk12@gmail.com

1 University Centre for Research and Development, Chandigarh University, Mohali, India

2 Department of Mechanical Engineering, Chandigarh University, Mohali, India

3 Department of Civil Engineering, University of Salerno, Salerno, Italy

(PMMA), and wood fiber (WF) has been prepared using the FFF process. The best mechanical properties were attained when PMMA and WF were reinforced into PLA having ratio 8:2 (mass ratio), and tensile strength and bending strength increased by 4.60% and 26.54% [21]. The addition of 1% ZnO nanofiber in PLA thermoplastic matrix has resulted in lesser thermal stability as compared to virgin PLA. However, the ZnO addition has resulted in higher crystallinity of nanocomposites [22]. To investigate the effects of reinforced particles on stiffness, PLA, bronze (Br)-filled PLA (PLA-Br), and silver (Ag)-filled PLA (PLA-Ag) were used in the FFF process. Results depicted that reinforcement of Br into PLA increased the elastic stiffness to 10% and 27% when printed at 0° and 90°, respectively. For Ag-filled PLA composites, the stiffness increased to 103% when printed at 90° [23]. It has been reported that the addition of separated continuous carbon (SCC) fiber increased the tensile strength and bending strength by 214% and 167%, respectively [24]. The quality of parts manufactured by FFF-based AM is highly dependent upon the post-processing. The PLA was reinforced with carbonized cellulose nanofibers (CCNFs), and it was observed that microwave annealing as a post-treatment reduced the standard time for post-processing and increased the mechanical strength [25]. The ABS matrix filled with multiwall carbon nanotubes (MWCNTs) as reinforcement enhanced the tensile strength by 288% [26]. Some of the relevant studies for the FFF process validated that reinforcement of particles in the thermoplastic matrix significantly improved the mechanical, thermal, morphological, rheological, and shape memory properties [27–29].

The reinforcement of metallic particulate is one of the conventional methods of modifying the mechanical/surface properties of the polymeric materials. Previous researchers have worked on the different metallic particles reinforced with thermoplastic composite materials for AM applications [23–29]. The reinforcement of metallic particles in thermoplastics is required pre-processing like: mechanical/chemical blending and extrusion process, which increases the processing time and overall manufacturing cost. In this study, the Al microfilm has been sprayed in-between the layers of PLA during the FFF process as a reinforcement material. This process has eliminated the requirement of the extrusion process for the reinforcement of metallic particles. The 3D printed structures manufactured by the FFF process are subjected to compressive testing for investigation of the role of microfilms and process variables. The results of the present study are supported by SEM, EDS, and DSC analysis.

2 Experimentation

2.1 Materials and methods

The feedstock filament of PLA (Manufacturer: Shenzhen Sunhokey Electronics Co., Ltd, China) having 1.75 ± 0.05 mm (diameter) size has been used in this study for the preparation of samples as per ASTM D 695 (see Fig. 1) [30]. The 99.9% commercially pure Al spray has been used for the deposition of microfilm in-between additive layers. In this study, the Al microfilm thickness of 50 µm with 1.15 mm/cm³ density has been used (manufacturer: Wurth India Ltd.). The Al spray is compressed with the mixture of acrylate–alkyd resin and is recommended for use up to 250 °C of a base temperature.

It has been claimed by the manufacturer that depositing the Al microfilm on the solid surface by 150 mm distance in one complete back and forth motion can deposit the microfilm with a thickness of 50 µm [31]. In present experimentation, the spray was done manually, one complete expel (one complete back and forth motion) of Al spray has deposited on PLA surface, and the average amount of Al microfilm weighted in one complete expel was 60 mg during pilot experimentation. Pilot experimentation was conducted three times for better accuracy and weighed the amount of microfilm deposited. Weight of microfilm was observed in pilot

Fig. 1 Design of compressive test specimen prepared as per ASTM D 695 standards (dimensions: 12.70 mm diameter and 25.40 mm length)
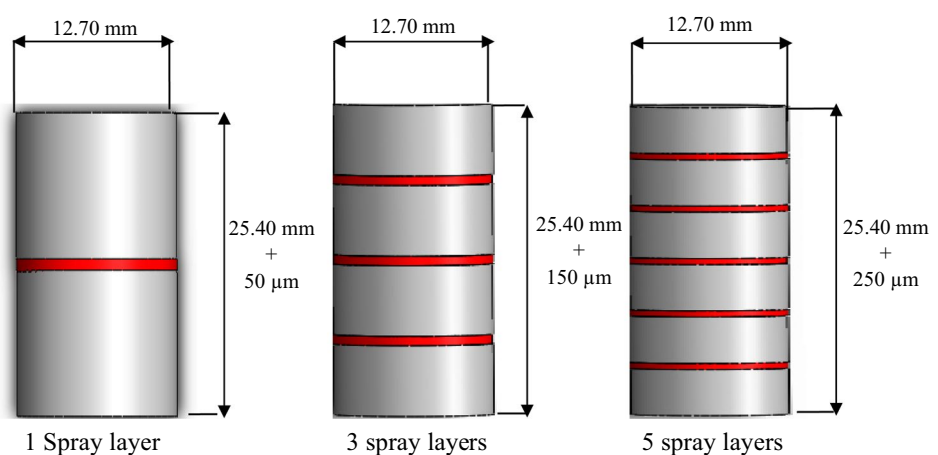
test for confirming the fact that aluminum can is spraying equal amount of aluminum in every spray.

2.2 FFF process

The fabrication was done using commercial FFF setup of Prusa i3 (model: MK2; maximum extruder temperature 283 °C and bed temperature: 135 °C). For slicing of ASTM D 695 design structures, commercial Ultimaker Cura 4.5 software has been used. The fill pattern of rectilinear type has been chosen for experimentation. The set of a total of 9 experiments has been performed. The Al spray was deposited on structures that act as microfilm on the structures. A PLA sample (without microfilm) of ASTM D 695 has also prepared on the standard FFF setting (100% infill and 100 °C bed temperature) for comparison of mechanical properties with microfilm reinforced samples. There are 3 input process variables selected for this study, namely no. of microfilm spray (1, 3, and 5 microfilms), bed temperature (60, 80, and 100 °C), and infill percentage (40, 70, and 100%). These levels of input process variables have been selected based upon the fact that during pilot experimentation, these levels have resulted in better dimensional accuracy. Previous studies suggested there is no direct relationship between the bed temperature and infill percentage in the FFF process. It has reported that FFF being performed above the glass transition temperature results in increased adhesion force between the layers; it increases the tendency for better sticking [32]. Also, increasing the bed temperature to a certain limit increases the tensile and flexural strength but started to decrease after crossing this limit due to excessive heat [33]. Table 1 shows the design of the experiment as per the Taguchi L9 orthogonal array.

The depositions of 1, 3, and 5 microfilms have been controlled by halting the FFF process at regular intervals. For example, for deposition of 1 microfilm in-between PLA surface, the FFF process was paused (after 50% part was manufactured) for 20 s, and then, spray of Al was deposited. Afterward, the FFF process was resumed to complete the rest of 50% fabrication. A similar approach was involved in the deposition of 3 and 5 microfilms layers. The spray interval for different Al layer is shown in Table 2. The rectilinear fill pattern was used for the fabrication of PLA structures. In the case of low infill percentage structures (40% and 70%), it has been observed that the microfilm layer directed in the voids/spaces/hole. But in case of structures having 100% infill, the microfilms were formed on the surface of the structure and in-between the layers of the part. As per ASTM D 695, in cylindrical form, the diameter of the compressive specimen is 12.7 mm, and the length is 25.4 mm. So, considering the layer height of 0.1 mm, a total of 254 number of layers were prepared. The spray was performed after extrusion of every 127, 63, and 42 layers in 1, 3, and 5 microfilms reinforced structures, respectively. The Z-axis or nozzle is controlled through CNC programming (by slicing software) to move upward after every layer formation during the FFF. The height of the microfilm is considered as very small as compared to the structure's height, so it was not considered as the part of the slicing program. Figure 2 shows the spraying strategy for the deposition of microfilm in-between PLA layers by FFF.

2.3 Mechanical testing

The mechanical properties (compressive strength at the peak, compressive strength at break, percentage compression at the peak, percentage compression as break, and modulus of toughness) of FFF parts were evaluated by using the universal testing machine (make: Shanta Engineering, India; maximum capacity: 5000 N). The compressive test was controlled at 50 mm/min compression speed.

2.4 Thermal analysis

DSC is one the most important observations which examines the thermal behavior of the polymers/metal/nonmetals/ alloys. In this study, the endothermic DSC examination was being performed in the range of 30–250 °C with a heating rate of 10 °C/min under an inert atmosphere of N_2 gas supply of 50 ml/min. The exothermic DSC examination was
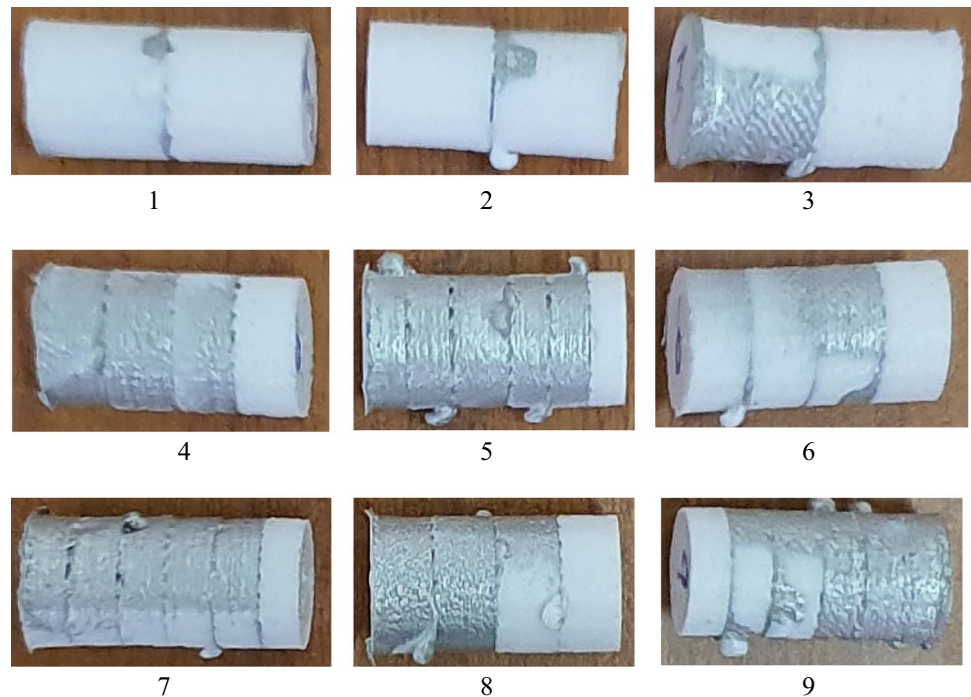
Table 1 Design of experiment as per Taguchi L9 orthogonal array

Exp no.	No. of layers	Infill percentage (%)	Bed temperature (°C)
1	1	40	60
2	1	70	80
3	1	100	100
4	3	40	80
5	3	70	100
6	3	100	60
7	5	40	100
8	5	70	60
9	5	100	80

Table 2 Spray strategy for the deposition of microfilm in-between PLA layers by FFF

No. of microfilm layers sprayed	Spraying intervals (process) (%)	Spraying intervals (layers)
1	50	127
3	25	63
5	17	42

Fig. 2 3D printed compression samples as per ASTM D 695

2.5 Morphology

The morphological analysis using the SEM apparatus (model: Jeol IT500) has been performed at X30 magnification. The fractured regions of samples (reinforced with microfilms) were compared with the standard sample of PLA. The SEM micrographs have been taken under 15 V power supply on vacuum mode (high vacuum). The EDS extension software of SEM setup has been used in this study for investigation of mass and the elemental fraction of the samples prepared with FFF. The EDS analysis has been performed at the fractured region of samples to investigate the presence of different elements.

## 2.6 Optimization process and methodology

The part prepared by the FFF process has been subjected to mechanical testing in the form of compressive strength at the peak, compressive strength at break, percentage compression at the peak, percentage compression as break,

performed in the range of 250–30 °C at − 10 °C/min under an inert atmosphere of N_2 gas supply of 50 ml/min. It should be noted that microfilm reinforced samples were crushed into powder form by using cryo-milling at − 196 °C. The powdered samples were preheated up to 90 °C for removing any thermal history associated in the form of contamination or additives. The process was repeated in two consecutive cycles to investigate the thermal stability and effects of heat exposure to various samples.

and modulus of toughness. Considering the maximization for mechanical properties, the optimization study has been performed to identify the best parametric settings. The methodology for the implementation of the optimization process is depicted in Fig. 3.

In the present study, the combination of analytic hierarchy process (AHP) and technique for order of preference by similarity to ideal solution (TOPSIS) has been used for the optimization of process parameters to attain maximum compressive properties of reinforced PLA structures. The step-by-step implementation of the TOPSIS–AHP process has been discussed in detail.

2.6.1 Selection of degree of preference

The degree of preference or intensity of the decision maker in the choice of each pair-wise comparison used in this model is quantified on a scale of 1–9. This scaling process can then be translated in priority weight (scores) for comparison of alternatives. Even numbers (2, 4, 6, 8) can be used to represent compromises among the preference above. In the present case, the mechanical properties such as compressive strength at the peak, compressive strength at break, percentage compression at the peak, percentage compression break, and modulus of toughness have been investigated. Thus, each response parameter of compressive strength is assigned a weight or score according to priority.
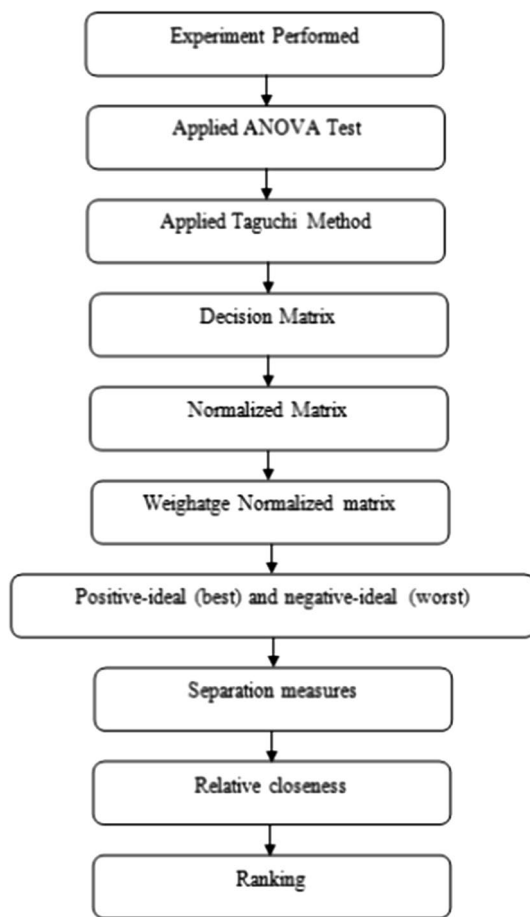
Fig. 3 An optimization approach for the selection of process parameters

2.6.2 Pair-wise comparison of different sub-objectives

Pair-wise matrix is formed between the response variables. The experts were asked to give rating to the importance of variables on the 9-point Satty's scale. The importance of *i*th sub-objective compared with *j*th sub-objectives is calculated (see Table 3).

2.6.3 Weightage of compression properties

The relative importance is given to each response parameter which further depends upon area of application. In the present study, the composite structures of PLA reinforced with Al spray are manufactured, which would be subjected to compressive loading of aerospace and automobile components. As the peak compressive strength is paramount and is required to be maximized, maximum weightage (40%) is given to this parameter. Similarly, for the present application area, minimum importance is given to toughness, and hence, only 8% weightage is given to this parameter. The preferences of weightage of mechanical properties are arranged in order from higher to lesser as compressive strength at peak, compressive strength at break, percentage compression at peak, percentage compression break, and modulus of toughness (see Table 4).

The TOPSIS was first developed by Hwang and Yoon [34]. According to this technique, the best alternative would be the one that is nearest to the positive-ideal solution and farthest from the negative-ideal solution [35]. In short, the positive-ideal solution is composed of all best values attainable from the criteria, whereas the negative-ideal solution consists of all worst values attainable from the criteria. Literature reveals that researchers have successfully implemented an integrated AHP–TOPSIS method to get reliable results. The applications of TOPSIS have been demonstrated in various domains such as tuning of En 25 Steel [36], CNC machining [37], machining of GFRP polyester composites [38], self-compacting concrete

Table 4 Weightage of compressive properties

Attributes	Priority weight
Compressive strength at peak (MPa)	0.40
Compressive strength at break (MPa)	0.21
Percentage compression at Peak (%)	0.18
Percentage compression at break (%)	0.12
Modulus of toughness (MPa)	0.08

Table 3 Comparison of *i*th sub-objective with *j*th sub-objectives

	Compressive strength at peak (MPa)	Compressive strength at break (MPa)	Percentage compression at peak (%)	Percentage compression at break (%)	Modulus of toughness (MPa)
Compressive strength at peak (MPa)	1	2	3	3	4
Compressive strength at break (MPa)	1/2	1	1	2	3
Percentage compression at peak (%)	1/3	1	1	2	2
Percentage compression at break (%)	1/3	1/2	1/2	1	2
Modulus of toughness (MPa)	1/4	1/3	1/2	1/2	1

[39], and abrasive water jet cutting [40] for optimization of process parameters during turning of EN25 steel.

Initially, the values of normalized matrix r_{ij} are calculated as given in the formulae mentioned below [34, 35]:

$$r_{ij} = a_{ij} / \left(\sum_{i=1}^{n} a^2 ij \right)^{0.5} \tag{1}$$

In the second step, the weightage to a normalized matrix is entered. The normalized matrix is multiplied with weightage assign to output parameters.

In the next step, determination of the positive-ideal (best) and negative-ideal (worst) solutions is done. The positive-ideal (best) and negative-ideal (worst) solutions can be expressed as [34, 35];

$$V^+ = \left\{ \left(\overset{max}{\underset{i}{\sum}} V_{ij} / j \in J \right), \left(\overset{min}{\underset{i}{\sum}} V_{ij} / j \in J' \right) / i = 1, 2, 3, \dots, N \right\},$$
$$= \{ V_1^+, V_2^+, V_3^+, V_4^+, \dots V_M^+ \} \tag{2}$$

$$V^- = \left\{ \left(\overset{min}{\underset{i}{\sum}} V_{ij} / j \in J \right), \left(\overset{max}{\underset{i}{\sum}} V_{ij} / j \in J' \right) / i = 1, 2, 3, \dots, N \right\},$$
$$= \{ V_1^-, V_2^-, V_3^-, V_4^-, \dots V_M^- \} \tag{3}$$

In the last step, the calculation of the separation measures is performed. The separation measure has been computed using the n-dimensional Euclidean distance. The separation of each alternative from the positive-ideal solution and the negative-ideal solution is given by the following equations.

$$S_1^+ = \left\{ \sum_{j=1}^{M} (V_{ij} - V_j^+)^2 \right\}^{0.5} \tag{4}$$

And,

$$S_1^- = \left\{ \sum_{j=1}^{M} (V_{ij} - V_j^-)^2 \right\}^{0.5} \tag{5}$$

The AHP–TOPSIS method is the most commonly used multi-criteria decision-making method. In the present work, the AHP method is used to provide subjective weights to response parameters, and the AHP weights are used in the TOPSIS method to provide ranking to parameters.

3 Results and discussion

3.1 Mechanical properties

Table 5 shows the compressive properties of microfilm reinforced structures of PLA composites. The maximum compressive strength has been measured during experiment no. 5 (parametric combination: 3 microfilms, 70% infill, and 100 °C bed temperature) due to the fact that, on this parametric combination, maximum layer diffusion has been experienced. The intermediate porous structure with 70% infill has promoted the microfilm deposition and made perfect entrapment of layers under a high bed temperature of 100 °C. It has also noticed that high bed temperature increases the bond strength (verified by observations of compressive strength). On the other hand, the minimum compressive strength was measured during experiment no. 1 (parametric combination: 1 microfilm, 40% infill, and 60 °C bed temperature) due to the fact that an insignificant microfilm layer, infill percentage, and bed temperature were unable to diffuse the additive

Table 5 Compressive properties of microfilm reinforced 3D printed structures

Exp. No.	Compressive strength at peak (MPa)	Compressive strength at break (MPa)	Percentage compression at peak (%)	Percentage compression at break (%)	Modulus of toughness $= \frac{1}{2} \times$ stress $\times$ strain. (MPa)
1	21.76 ± 0.25	19.58 ± 0.25	5.00 ± 0.00	17 ± 0.00	1.664.00
2	21.88 ± 0.26	19.7 ± 0.26	6.00 ± 0.00	13 ± 0.00	1.28.00
3	22.4 ± 0.31	20.16 ± 0.31	5.00 ± 0.00	12 ± 0.00	1.209.00
4	25.28 ± 0.42	22.75 ± 0.42	3.00 ± 0.00	3 ± 0.00	0.341.00
5	26.83 ± 0.48	24.15 ± 0.48	3.00 ± 0.00	3 ± 0.00	0.362.00
6	25.55 ± 0.42	22.99 ± 0.42	4.00 ± 0.00	4 ± 0.00	0.459.00
7	25.06 ± 0.49	22.55 ± 0.49	5.00 ± 0.00	5 ± 0.00	0.563.00
8	26.21 ± 0.58	23.59 ± 0.58	4.00 ± 0.00	4 ± 0.00	0.471.00
9	26.49 ± 0.74	23.84 ± 0.74	3.00 ± 0.00	3 ± 0.00	0.357.00
PLA	22.12 ± 0.42	19.93 ± 0.42	4.00 ± 0.00	7 ± 0.00	0.697.00

layers efficiently. It should be noted that the parts prepared by 3 and 5 microfilm layers have attained higher compressive strength as compared to virgin PLA. Sample 5 and sample 9 have showed almost similar results, even though both the samples have different number of layers (i.e., 3 and 5). Sample 5 has shown good mechanical properties due to the fact that bed temperature of 100 °C was used during fabrication, and the same results are also being observed by many researchers that increase in bed temperature enhances the mechanical properties of printed specimen [41]. Infill density also has significant effect on mechanical properties; in case of single polymer matrix with increase in infill density, compressive and tensile strength increases. It is due to the fact that higher infill density means more material deposited, and this higher concentration of material can provide more resistance to the deformation [42]. The reason for similar mechanical properties of sample 5 and sample 9 can be predicted from the fact that both infill percentage and bed temperature have played a crucial role. In case of the sample 5, it is the combination of intermediate infill percentage (70%) and maximum bed temperature (80 °C), whereas in case of sample 9, the experimental condition is maximum infill (100%) and intermediate bed temperature (80 °C). Due to the similar relative variation over infill percentage and bed temperature, the results are obtained almost similar in case of sample 5 and sample 9.

Figure 4 shows the stress versus strain curves of compressive properties. The modulus of toughness is the measure of resistance to deformation of the component; it matters a lot when the application area of study is crash resistance of composite structures. The maximum modulus of toughness was noted in the case of experiment no. 1 (modulus of toughness: 1.664 MPa) since the percentage compression was 17% in this sample. Although the sample of experiment 5 has exhibited maximum compressive strength, due to the

lower compressive deformation, the modulus of toughness was comparatively less (modulus of toughness: 0.362 MPa).

3.2 Morphological analysis

The SEM images for fractured surfaces of sample 1 (minimum compressive strength), sample 5 (maximum compressive strength), and PLA sample without microfilm are shown in Fig. 5. The arrow represents the direction of compressive forced acted on the surface of PLA structures. In sample 1 and sample 5, compression force is applied uniaxially along one direction, due to which decrease in length in the same direction occurs. It has been observed that the additive layers of sample 1 have crossed to each other by compression; it is due to the fact that the infill percentage of sample 1 is only 40%. The less infill in sample 1 has facilitated the longer compression, i.e., up to 17%. In the case of sample 5, due to the intermediate infill percentage (infill: 70%) and intermediate microfilm layers (3 layers) and maximum bed temperature (100 °C), the samples yielded maximum compressive strength due to tight bond formations. It should be noted that, due to the tight sticking between the layers, the compression was experienced only up to 3% in the case of sample 5. Sample 10 or unsprayed sample of PLA (without microfilm) material was prepared under 100 °C bed temperature, and 100% infill density, and it has been analyzed under 30× magnification to see the fusion between the layers. It has been deduced that due to 100% infill density and 100 °C bed temperature, both compressive strength and compression percentages are in mid-range. It means that both the factors, reinforcement of microfilm and bed temperature, are the important parameters that must be controlled for the excellent adhesion of additive layers.

Figure 6 shows the morphology of fractured surface in 3D render view and surface roughness plots of sample 1 (1

Fig. 4 Stress versus strain curves for compressive properties
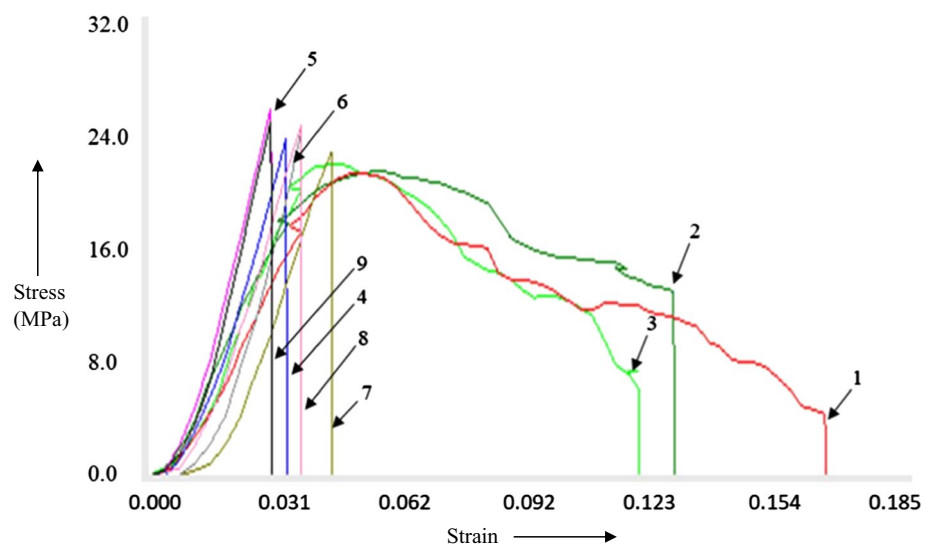
Fig. 5 SEM observation of fractured surface at ×30 magnification
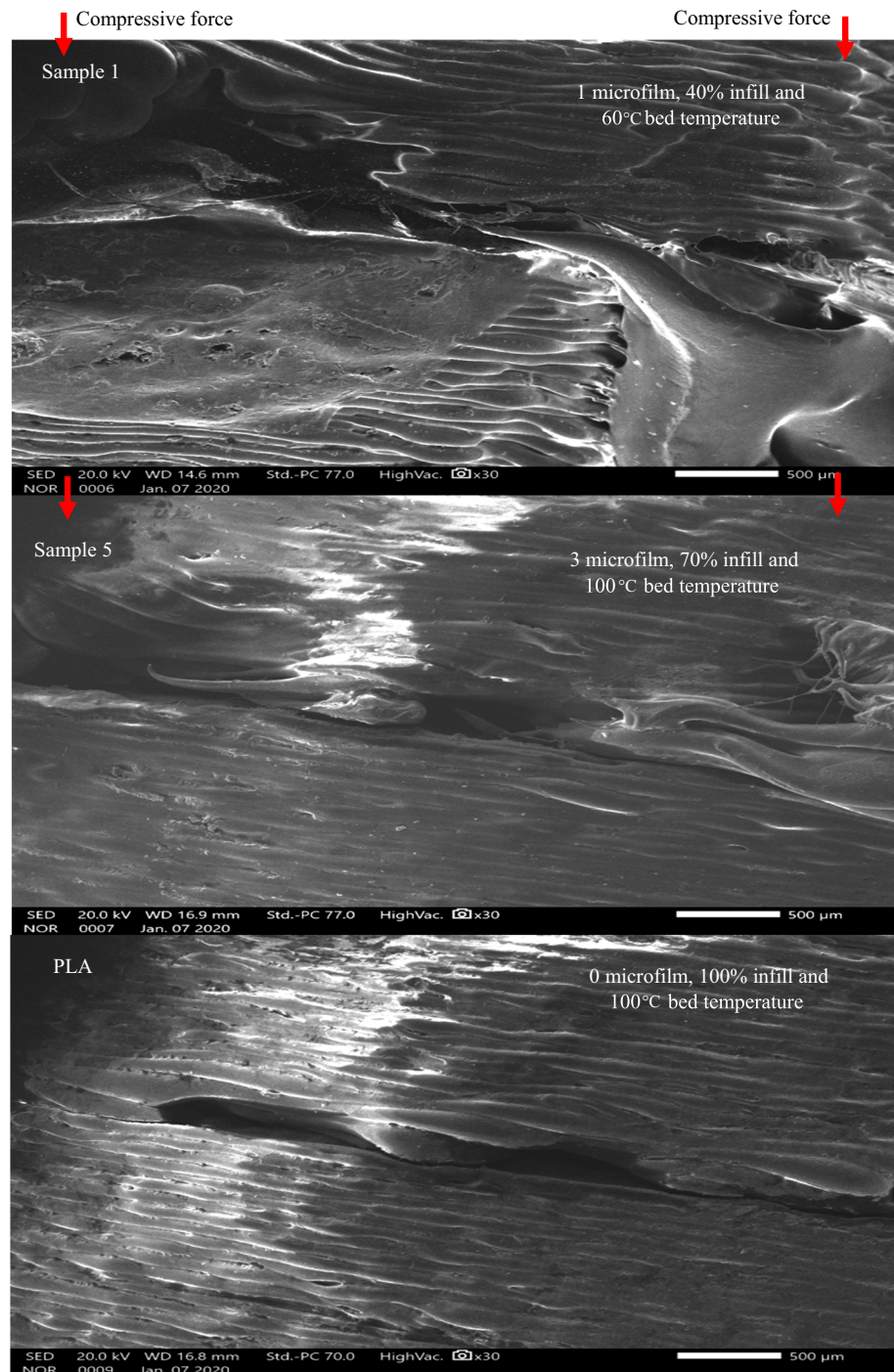

spray layer, 40% infill density and 60 °C bed temperature), sample 5 (3 spray layers, 70% infill density, and 100 °C bed temperature), and unsprayed PLA sample. For sample 1, the surface roughness measured is 21.57 μm, the surface roughness value of sample 1 is greater than both the sample 5 (having surface roughness 20.90 μm) and unsprayed PLA (having surface roughness 16.58 μm).

The reason for the higher surface roughness of sample 1 is due to the fact that it was prepared under 40% of infill density. Due to low infill density, sample 1 has attained more pores and sharp edges than the other samples. Higher surface roughness shows that it experienced more compression under high compressive loading. In sample 5, the value of surface roughness is comparatively lesser due to the 70% infill density and 3 spray of Al microfilm. The surface roughness of unsprayed PLA prepared under 100% infill density, and 100 °C bed temperature was observed lesser (16.58 μm) as compared to sample 1 and sample 5.
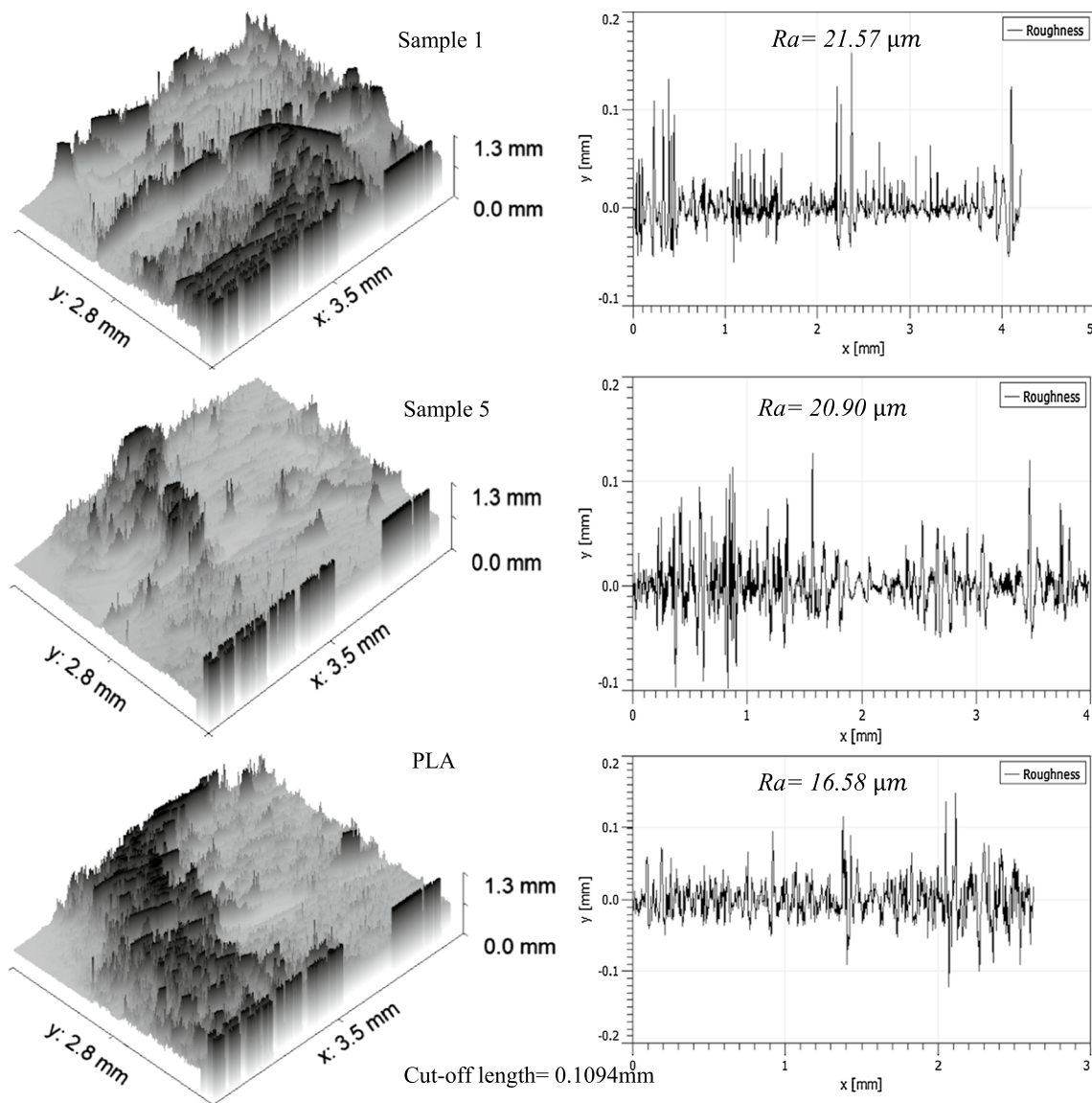
Fig. 6 3D morphology of fracture surface and corresponding surface roughness graphs

Figure 7 shows the EDS plots of sample 1 and sample 5. The concentration of Al in sample 1 was 0.69% as elemental, and the mass fraction is 1.28%. In sample 5, since the no. of layers are 3 times than the sample 1, the value of the element and the mass fraction is almost more than three times as compared to sample 1. The small deflection in these values is due to the fact that there are some chances of uneven sprayed layers of Al.

3.3 Thermal analysis

Figure 8 shows the DSC plots of PLA (sample 1), PLA + 1 microfilm (sample 2), PLA + 3 microfilm (sample 3), and PLA + 5 microfilm (sample 4) samples. It has been noticed that the addition of microfilm in the PLA layers has increased the glass transition temperature as it was 58.62 °C for PLA, 58.72 °C for PLA + 1 microfilm, 60.47 °C for PLA + 3 microfilm, and 62.48 °C for PLA + 5 microfilm. So, reinforcement of the Al microfilm has led to a decrease in the tendency to deform the materials.

In the second cycle, the glass transition temperature of PLA, PLA + 1 microfilm, PLA + 3 microfilm, and PLA + 5 microfilm has been found 59.62 °C, 60.58 °C, 61.52 °C, and 62.42 °C, respectively, which varied to very insignificant loading. This tendency to insignificant variation of glass transition temperature over second cycle shows that material is thermally stable in nature. On the other hand, similar observations have been found in the case of normalized heat capacity where it was not changed to a great extent, which means the materials are thermally stable.
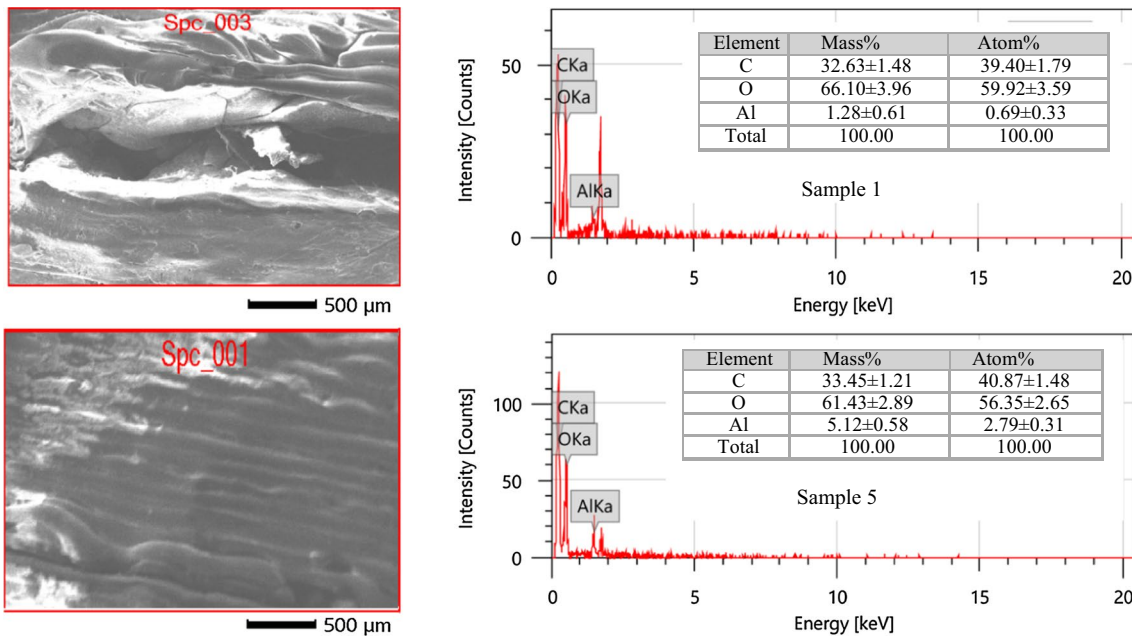
Fig. 7 EDS analysis of sample 1 (1 microfilm layer) and sample 5 (3 microfilm layers)
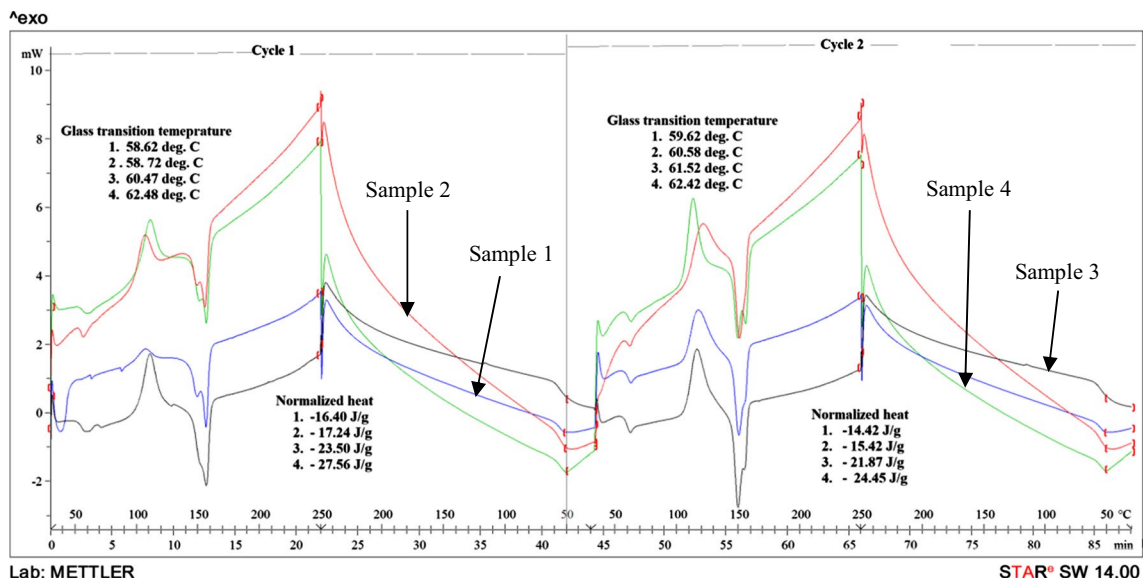

Fig. 8 DSC plots of samples

3.4 Optimization of process parameters

The TOSIS method has been used to optimize the input process parameters of the FFF. The input process parameters have been optimized by taking the values of the compressive properties. Initially, the values of normalized matrix r_{ij} are calculated as given in the formulae in Eq. 1 (Table 6):

In the second step, the weightage to a normalized matrix is entered. The normalized matrix is multiplied with weightage assign to output parameters. In the present work, the equal weightage has been assigned to output parameters (see Table 7).

In the next step, determination of the positive-ideal (best) and negative-ideal (worst) solutions is done. The positive-ideal (best) and negative-ideal (worst) solutions have been calculated using Eqs. 2 and 3 (see Table 8).

Table 6 Normalize matrix for compressive properties

Exp no.	Compressive strength at peak (MPa)	Compressive strength at break (MPa)	Percentage compression at peak (%)	Percentage compression at break (%)	Modulus of toughness (MPa)
1	0.29	0.29	0.38	0.65	0.63
2	0.29	0.29	0.46	0.49	0.48
3	0.30	0.30	0.38	0.45	0.46
4	0.34	0.34	0.23	0.11	0.13
5	0.36	0.36	0.23	0.11	0.18
6	0.34	0.34	0.30	0.15	0.17
7	0.34	0.34	0.38	0.19	0.21
8	0.35	0.35	0.30	0.15	0.18
9	0.36	0.33	0.23	0.11	0.13

Table 7 Weightage of compressive properties

Exp no.	Compressive strength at peak (MPa)	Compressive strength at break (MPa)	Percentage compression at peak (%)	Percentage compression at break (%)	Modulus of toughness (MPa)
1	0.12	0.06	0.07	0.08	0.05
2	0.12	0.06	0.08	0.06	0.04
3	0.12	0.06	0.07	0.05	0.04
4	0.14	0.07	0.04	0.01	0.01
5	0.15	0.08	0.04	0.01	0.01
6	0.14	0.07	0.06	0.02	0.01
7	0.14	0.07	0.07	0.02	0.02
8	0.14	0.08	0.06	0.02	0.01
9	0.14	0.08	0.04	0.01	0.01

Table 8 The positive-ideal (best) and negative-ideal (worst) solutions

Output parameters	Positive-ideal	Negative-ideal
Compressive strength at peak (MPa)	0.14	0.12
Compressive strength at break (MPa)	0.08	0.06
Percentage compression at peak (%)	0.08	0.04
Percentage compression at break (%)	0.08	0.01
Modulus of toughness (MPa)	0.05	0.01

Table 9 Separation of each alternative from the positive-ideal solution and negative-ideal solution

Exp no.	Positive separation measure	Negative separation measure
1	0.03	0.08
2	0.03	0.07
3	0.04	0.06
4	0.08	0.02
5	0.09	0.03
6	0.08	0.03
7	0.07	0.04
8	0.07	0.03
9	0.09	0.03

The separation of each alternative from the positive-ideal solution and the negative-ideal solution has been calculated using Eqs. 4 and 5 (see Table 9).

Table 10 shows the relative closeness values and ranking of each experiment.

The AHP–TOPSIS method is the most commonly used multi-criteria decision-making method. In the present work, the AHP method is used to provide subjective weights to response parameters, and the AHP weights are used in the TOPSIS method to provide ranking to parameters. The result of the TOPSIS method showed that experiment no. 1 has the highest value of relative closeness and followed by experiment no. 2; therefore,

Table 10 Relative clearance value

Exp no.	Relative closeness values	Ranking
1	0.70	1
2	0.64	2
3	0.58	3
4	0.20	9
5	0.27	7
6	0.27	6
7	0.35	4
8	0.29	5
9	0.25	8

experiment no. 1 and experiment no. 2 are placed at rank 1 and rank 2, respectively.

4 Conclusions

Following conclusions have been made from the present study:

- The mechanical properties of the Al spray reinforced PLA parts fabricated by FFF are greatly influenced by varying bed temperature and infill percentage. The porous structure with 70% infill has supported the microfilm deposition and made perfect entrapment of layers under high bed temperature of 100 °C. It has been observed that high bed temperature increases the bond strength (verified by observations of compressive strength). On the other hand, the minimum compressive strength is attained during experiment no. 1 (parametric combination: 1 microfilm, 40% infill, and 60 °C bed temperature) due to the fact that insignificant microfilm layer, infill percentage, and bed temperature are unable to diffuse the additive layers efficiently.

- The glass transition temperature of PLA, PLA + 1 microfilm, PLA + 3 microfilm, and PLA + 5 microfilm has been found 59.62 °C, 60.58 °C, 61.52 °C, and 62.42 °C, respectively, in second thermal cycle, which varied insignificantly as compared to first thermal cycle. This tendency to insignificant variation of glass transition temperature over second cycle shows that material is thermally stable. Similar observations have been found in the case of normalized heat capacity where it was not changed to a great extent, which means the materials are thermally stable. The addition of microfilm does not affect the thermal stability of the materials. Based upon these facts, parts prepared by this hybrid FFF technique can be applied in various structures for automobile and aerospace applications.

- The TOPSIS–AHP method has been implemented to attain maximum compressive strength at peak and compressive strength at break with 40% and 21% weightage, respectively. The result of TOPSIS method suggested that to achieve the highest value of response parameters with subjective weights (0.40 0.21 0.18 0.12 0.08) the values of the number of microfilm layers, infill percentage, and bed temperature should be 1, 40%, and 60 °C, respectively (experiment no. 1).

References

1. Attaran M (2017) The rise of 3-D printing: the advantages of additive manufacturing over traditional manufacturing. Bus Horiz 60(5):677–688
2. Mathias D, Snider C, Hicks B, Ranscombe C (2019) Accelerating product prototyping through hybrid methods: coupling 3D printing and LEGO. Des Stud 62:68–99
3. Singh S, Prakash C, Ramakrishna S (2019) 3D printing of polyether-ether-ketone for biomedical applications. Eur Polym J 114:234–248
4. Tilford T, Stoyanov S, Braun J, Janhsen JC, Burgard M, Birch R, Bailey C (2018) Design, manufacture and test for reliable 3D printed electronics packaging. Microelectron Reliab 85:109–117
5. Ordoñez E, Gallego JM, Colorado HA (2019) 3D printing via the direct ink writing technique of ceramic pastes from typical formulations used in traditional ceramics industry. Appl Clay Sci 182:105285
6. Ford S, Minshall T (2019) Invited review article: where and how 3D printing is used in teaching and education. Addit Manuf 25:131–150
7. Liu Z, Lei Q, Xing S (2019) Mechanical characteristics of wood, ceramic, metal and carbon fiber-based PLA composites fabricated by FDM. J Mater Res Technol 8(5):3741–3751
8. Li M, Chen AN, Lin X, Wu JM, Chen S, Cheng LJ et al (2019) Lightweight mullite ceramics with controlled porosity and enhanced properties prepared by SLS using mechanical mixed FAHSs/polyamide12 composites. Ceram Int 45(16):20803–20809
9. Krinitcyn M, Fu Z, Harris J, Kostikov K, Pribytkov GA, Greil P, Travitzky N (2017) Laminated object manufacturing of in situ synthesized MAX-phase composites. Ceram Int 43(12):9241–9245
10. ASTM (2012) Standard terminology for additive manufacturing technologies. ASTM International F2792-12a, West Conshohocken
11. Lay M, Thajudin NLN, Hamid ZAA, Rusli A, Abdullah MK, Shuib RK (2019) Comparison of physical and mechanical properties of PLA, ABS and nylon 6 fabricated using fused deposition modeling and injection molding. Compos B Eng 176:107341
12. Ni J, Ling H, Zhang S, Wang Z, Peng Z, Benyshek C et al (2019) Three-dimensional printing of metals for biomedical applications. Mater Today Bio 3:100024
13. Valino AD, Dizon JRC, Espera AH Jr, Chen Q, Messman J, Advincula RC (2019) Advances in 3D printing of thermoplastic polymer composites and nanocomposites. Prog Polym Sci 98:101162

14. Henke K, Treml S (2013) Wood based bulk material in 3D printing processes for applications in construction. Eur J Wood Wood Prod 71(1):139–141

15. Chen Z, Li Z, Li J, Liu C, Lao C, Fu Y et al (2019) 3D printing of ceramics: a review. J Eur Ceram Soc 39(4):661–687

16. Hassan M, Dave K, Chandrawati R, Dehghani F, Gomes VG (2019) 3D printing of biopolymer nanocomposites for tissue engineering: nanomaterials, processing and structure–function relation. Eur Polym J 121:109340

17. Dankar I, Haddarah A, Omar FE, Sepulcre F, Pujolà M (2018) 3D printing technology: the new era for food customization and elaboration. Trends Food Sci Technol 75:231–242

18. Singh R, Singh N, Fabbrocino F, Fraternali F, Ahuja IPS (2016) Waste management by recycling of polymers with reinforcement of metal powder. Compos B Eng 105:23–29

19. Kim DY, Kim JH, Kim HY, Kim WC (2018) Comparison and evaluation of marginal and internal gaps in cobalt–chromium alloy copings fabricated using subtractive and additive manufacturing. J Prosthodont Res 62(1):56–64

20. Patton MV, Ryan P, Calascione T, Fischer N, Morgenstern A, Stenger N, Nelson-Cheeseman BB (2019) Manipulating magnetic anisotropy in fused filament fabricated parts via macroscopic shape, mesoscopic infill orientation, and infill percentage. Addit Manuf 27:482–488

21. Wan L, Zhang Y (2018) Jointly modified mechanical properties and accelerated hydrolytic degradation of PLA by interface reinforcement of PLA-WF. J Mech Behav Biomed Mater 88:223–230

22. Nonato RC, Mei LHI, Bonse BC, Chinaglia EF, Morales AR (2019) Nanocomposites of PLA containing ZnO nanofibers made by solvent cast 3D printing: production and characterization. Eur Polym J 114:271–278

23. Alam F, Shukla VR, Varadarajan KM, Kumar S (2020) Microarchitected 3D printed polylactic acid (PLA) nanocomposite scaffolds for biomedical applications. J Mech Behav Biomed Mater 103:103576

24. Ye W, Lin G, Wu W, Geng P, Hu X, Gao Z, Zhao J (2019) Separated 3D printing of continuous carbon fiber reinforced thermoplastic polyimide. Compos A Appl Sci Manuf 121:457–464

25. Dong J, Huang X, Muley P, Wu T, Barekati-Goudarzi M, Tang Z et al (2020) Carbonized cellulose nanofibers as dielectric heat sources for microwave annealing 3D printed PLA composite. Compos B Eng 184:107640

26. Sezer HK, Eren O (2019) FDM 3D printing of MWCNT reinforced ABS nano-composite parts with enhanced mechanical and electrical properties. J Manuf Process 37:339–347

27. Kumar S, Singh R, Singh TP, Batish A (2020) Investigations for mechanical, thermal and magnetic properties of polymeric composite matrix for four-dimensional printing applications. J Braz Soc Mech Sci Eng 42(4):1–15

28. Francis V, Jain PK (2018) A filament modification approach for in situ ABS/OMMT nanocomposite development in extrusion-based 3D printing. J Braz Soc Mech Sci Eng 40(7):361

29. Monteiro JRL, d'Almeida JRM (2018) Evaluation of the mechanical performance of the creep behavior of a fiberglass repair after aging in oil. J Braz Soc Mech Sci Eng 40(7):346

30. Standard ASTM (2014) D638-14. Standard test method for tensile properties of plastics. https://www.astm.org/Standards/D638. Retrieved on 18 Aug 2020

31. Wurth India Ltd. https://eshop.wuerth.in/Perfect-aluminium-spray-matt-ALUSPR-PLUS-400ML/0893114115.sku/en/US/INR/. Retrieved on 15 May 2020

32. Spoerk M, Gonzalez-Gutierrez J, Sapkota J, Schuschnigg S, Holzer C (2018) Effect of the printing bed temperature on the adhesion of parts produced by fused filament fabrication. Plast Rubber Compos 47(1):17–24

33. Chadha A, Ul Haq MI, Raina A, Singh RR, Penumarti NB, Bishnoi MS (2019) Effect of fused deposition modelling process parameters on mechanical properties of 3D printed parts. World J Eng 16(4):550–559. https://doi.org/10.1108/WJE-09-2018-0329

34. Hwang CL, Yoon K (1981) Multiple attribute decision making: methods and applications. Springer, New York. https://doi.org/10.1007/978-3-642-48318-9

35. Shih HS, Shyur HJ, Lee ES (2007) An extension of TOPSIS for group decision making. Math Comput Model 45(7–8):801–813

36. Lan TS (2009) Taguchi optimization of multi-objective CNC machining using TOPSIS. Inf Technol J 8(6):917–922

37. Singh A, Datta S, Mahapatra SS (2011) Application of TOPSIS in the Taguchi method for optimal machining parameter selection. J Manuf Sci Prod 11(1–3):49–60

38. Balasubramaniyan S, Selvaraj T (2017) Application of integrated Taguchi and TOPSIS method for optimization of process parameters for dimensional accuracy in turning of EN25 steel. J Chin Inst Eng 40(4):267–274

39. Şimşek B, İç YT, Şimşek EH (2013) A TOPSIS-based Taguchi optimization to determine optimal mixture proportions of the high strength self-compacting concrete. Chemometr Intell Lab Syst 125:18–32

40. Yuvaraj N, Pradeep Kumar M (2015) Multiresponse optimization of abrasive water jet cutting process parameters using TOPSIS approach. Mater Manuf Process 30(7):882–889

41. Khatwani J, Srivastava V (2019) Effect of process parameters on mechanical properties of solidified PLA parts fabricated by 3D printing process. In: Kumar L, Pandey P, Wimpenny D (eds) 3D printing and additive manufacturing technologies. Springer, Singapore. https://doi.org/10.1007/978-981-13-0305-0_9

42. Torres J, Cotelo J, Karl J, Gordon AP (2015) Mechanical property optimization of FDM PLA in shear with multiple objectives. JOM 67(5):1183–1193